Spectrochimica Acta Part A: Molecular and Biomolecular Spectroscopy 251 (2021) 119434

Contents lists available at ScienceDirect

Spectrochimica Acta Part A: Molecular and Biomolecular Spectroscopy

journal homepage: www.elsevier.com/locate/saa

A QM/MM study of the conformation stability and electronic structure of the photochromic switches derivatives of DHA/VHF in acetonitrile solution

Marcelo Hidalgo Cardenuto [a], Henrique M. Cezar [a], Kurt V. Mikkelsen [b], Stephan P.A. Sauer [b], Kaline Coutinho [a], Sylvio Canuto [a,*]

[a] Instituto de Física, Universidade de São Paulo, Rua do Matão 1371, Cidade Universitária, 05508-090 São Paulo, Brazil
[b] Department of Chemistry, University of Copenhagen, Universitetsparken 5, 2100 Copenhagen, Denmark

HIGHLIGHTS

- Molecular photoswitches DHA/VHF were theoretically studied in acetonitrile solution.
- Sequential QM/MM was used to obtain the electronic absorption spectra.
- Conformational sampling of photoswitches was obtained with CBMC simulations.
- Free energy releases were obtained with Free Energy Perturbation in MM simulations.
- Most important solvent effect in the absorption spectra is the band broadning.
- Only explicit solvent provides the correct signal of the solvation free energy.

GRAPHICAL ABSTRACT

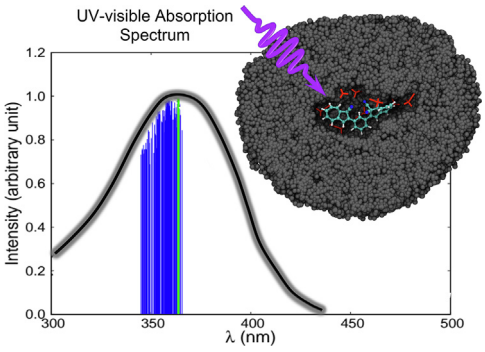

ARTICLE INFO

Article history:
Received 16 October 2020
Received in revised form 30 December 2020
Accepted 3 January 2021
Available online 6 January 2021

Keywords:
QM/MM method
Absorption spectroscopy
Electronic structure
Molecular
Photoswitches
Solvent effects

ABSTRACT

We present a detailed theoretical study of the electronic absorption spectra and thermochemistry of molecular photoswitches composed of one and two photochromic units of dihydroazulene (DHA)/vinylheptafulvene (VHF) molecules. Six different isomers are considered depending on the ring opening/closure forms of the DHA units. The solvent effect of acetonitrile is investigated using a sequential Molecular Mechanics/Quantum Mechanics approach. The thermochemical investigations of these photochromic molecules were performed using the Free Energy Perturbation method, and the simulations were performed using Configurational Bias Monte Carlo. We show that to open the 5-member ring of the DHA, there is no significant gain in thermal release of energy for the back reaction when a unit or two DHA units are considered. Overall, we found agreement between the solvation free energy based on Monte Carlo simulations and the continuum solvent model. However, the cavitation term in the continuum model is shown to be a source of disagreement when the non-electrostatic terms are compared. The electronic absorption spectra are calculated using TDDFT CAM-B3LYP/cc-pVDZ. Agreement with experiment is obtained within 0.1 eV, considering statistically uncorrelated configurations from the simulations. Inhomogeneous broadening is also considered and found to be well described in all cases.

* Corresponding author.
E-mail addresses: kaline@if.usp.br (K. Coutinho), canuto@if.usp.br (S. Canuto).

https://doi.org/10.1016/j.saa.2021.119434
1386-1425/

1. Introduction

Photochromic molecules have received much attention due to their widespread applicability in different fields of science and technology. The term photochromism is used to define the reversible changes in the physical or chemical properties of molecules or materials when stimulated by light [1–3]. These molecules presenting light-induced behavior are named photochromic compounds. An exceptional example are the molecular switches [4], a molecular scale electronic device capable of changing its properties when exposed to an external stimulus like radiation, temperature variations or environment effects. When they present light-induced switching, those molecules are known also as photoswitches. The possibility for practical applications as novel materials in interdisciplinary fields like data storage, information processing, molecular sensors and energy storage devices justifies the large interest in understanding the properties of these molecules. In particular the search for renewable energy sources is an increasingly important subject that brings together efforts to capture, store and release energy after its conversion into another form, like thermal energy [5]. Sunlight is a very abundant and clean energy source and many compounds are able to perform a process of absorption, photochemical conversion and storage of its energy, i.e., working as a battery. But, the search for good candidates maximizing their efficiency in this process is still a challenging task for both theoretical and experimental studies.

An interesting photochromic molecule is the dihydroazulene (DHA) and its derivative vinylheptafulvene (VHF), both shown in Fig. 1. The DHA undergoes a photoinduced ring-opening to the VHF form and a reversible thermally assisted ring-closure back to the DHA [6,7]. These opening/closure reactions enable these molecules to work in capture, storage and delivery energy processes. The incorporation of a variety of substituent groups covalently bound into DHA/VHF provides the possibility to tune the electronic properties of these molecules. Their absorption maximum is sensitive to the nature of the substituent as well as the solvent [8–11] in a domain of 350–490 nm.

The thermochemical properties of the DHA/VHF molecules (Gibbs free energy, for example) are particularly important. The Gibbs free energy is used to determine the barrier for the thermal back-reaction in the conversion of VHF to DHA and it is related to the energy storage capacity [10,11], which is a parameter guiding the design of solar heat battery systems. The electronic absorption spectra are also important because they allow the possibility of monitoring the opening/closure ring process in these compounds as their absorbance and wavelength change in time. Recently, a two DHA units molecule was proposed [12] and also a more complex group of molecules composed by two DHA units incorporating a macrocyclic ring system or DHA confined in cucurbituril host molecules were studied in experimental and theoretical works as well [13–20].

The practical applications of these compounds in molecular devices occur both in condensed phase and in polymeric matrix. Understanding the solvent effects on the properties of these molecules is hereby one of the important issues. The synthesis of photochromic molecules is normally solvent-assisted and the electronic properties are sensitive to each solvent. The theoretical procedure to treat the effect of solvents is not unique and an approach often used is to represent the solvent as a continuum, in which the main characteristic used is the dielectric constant. Although suitable and successful in many cases, the continuum approach presents some limitations with respect to local solvation details.

Here we intend to study the single units DHA and VHF, and also two units of DHA covalently linked by a benzene ring in acetonitrile solution. The solvent effects on spectroscopic properties of these molecules were studied by computational methods, but restricted to the acetonitrile continuum solvent approach [10–15]. Considering a discrete solvent approach, we study here the DHA photochromes as a prototype, and therefore, not as complex as the macrocyclic incorporated molecules [13–15]. To our knowledge there is no theoretical study considering the solvent effects explicitly with the aid of molecular mechanics approach on the electronic properties or free energy of these photochromes. This

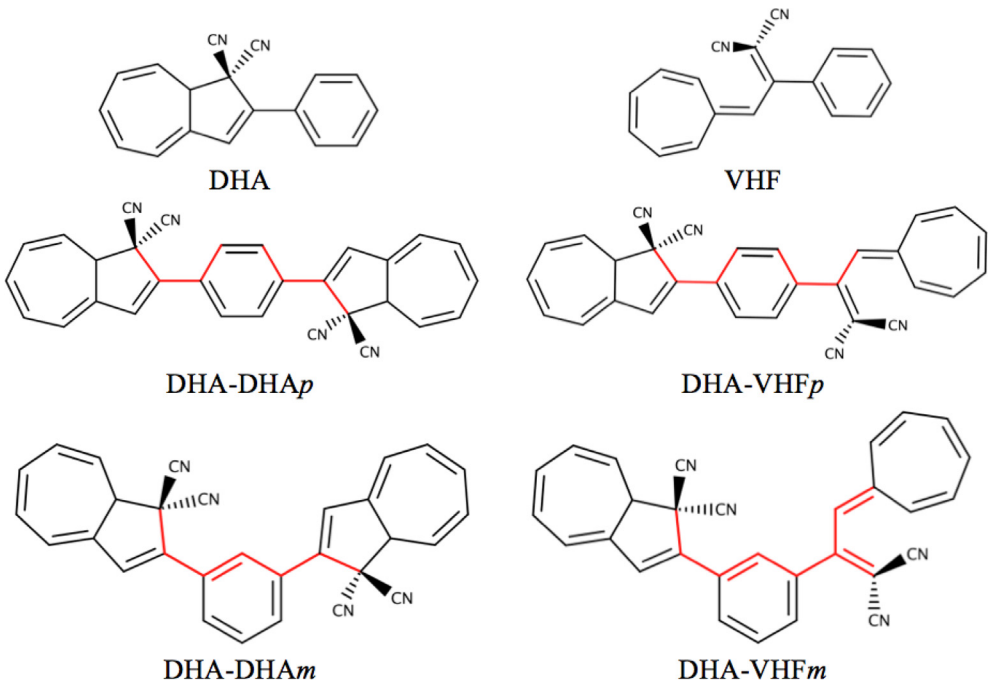

Fig. 1. Molecular structures of DHA, VHF and the DHA-DHA, DHA-VHF two-units molecules bounded in *para* (*p*) and *meta* (*m*) positions with respect to the central benzene ring. The colored red bonds represent the rotatable bonds, which are flexible during the simulations as discussed in the text.

study is timely and necessary to validate the use of acetonitrile continuum models for structural and electronic properties and mostly for free energy variations. Most of the experimental measurements of the photoswitch molecules are performed in acetonitrile solution, because organic nitrile-based solvents give high efficiency in photo-devices [4]. The hybrid QM/MM (Quantum Mechanics/Molecular Mechanics) approach is a good choice to include statistical information of the disordered nature of the solvent, at non-zero temperature, and also to consider the conformational changes caused by the solute–solvent interaction. In the case of electronic absorption spectra this allows to include the inhomogeneous contribution to band broadening.

Hence, we investigate the electronic absorption spectra and solvation free energies in a multiscale approach combining molecular mechanics and quantum mechanical calculations using the sequential method (S-QM/MM), successfully used in many cases [21–27] of spectroscopic and free energy calculations [28,29]. In the next section we present details of the methodology in Section 2 followed by the results in Section 3. Conclusions are presented in Section 4.

2. Computational procedures

2.1. Gas phase and continuum model QM calculations

The minimum energy geometries of the solutes or photochromes were optimized using quantum mechanics (QM) calculation within density functional theory with the hybrid exchange–correlation functional CAM-B3LYP functional [30] and correlation consistent basis sets, cc-pVDZ [31] in vacuum and in solution using the Polarizable Continuum Model (PCM) [32–34]. Besides the DHA and VHF monomers, four other molecules were optimized: dimers of the two photochromes, which we name DHA-DHA*p*, DHA-DHA*m*, DHA-VHF*p* and DHA-VHF*m*. These two-unit molecules are bounded by a benzene ring in the *para* (*p*) and *meta* (*m*) positions as shown in Fig. 1.

The optimized geometries obtained in vacuum or gas phase (X_{gas}) and in acetonitrile solution (X_{sol}) were compared and the difference in the electronic energy due to the geometry modification was obtained with QM calculation, $\Delta E_{geom} = E_{gas}(X_{sol}) - E_{gas}(X_{gas})$. The vibrational frequencies were also calculated, providing the Gibbs free energy for each molecule, in gas phase, $G_{gas}(X_{gas})$, and in solution, $G_{sol}(X_{sol})$. Therefore, zero-point energy, enthalpic and entropic corrections are taken into account in the Gibbs free energy. Considering the reaction X→Y that opens the 5-member ring changing X = DHA into Y = VHF, the difference of the free energy in gas was obtained with QM calculation, $\Delta G_{gas}(X_{gas} \rightarrow Y_{gas}) = G_{gas}(Y_{gas}) - G_{gas}(X_{gas})$. In solution, this free energy difference can be obtained directly as $\Delta G_{sol}(X_{sol} \rightarrow Y_{sol}) = G_{sol}(Y_{sol}) - G_{sol}(X_{sol})$, only when the geometries of X_{sol} and Y_{sol} have similar volumes leading to the neglect of the cavitation energy contribution. In other words, the Gibbs free energy obtained with QM calculation is incomplete, because it does not take into account the cavitation free energy term, G_{cav}. Therefore, when $G_{cav}(X_{sol}) \cong G_{cav}(Y_{sol})$, the difference in the cavitation free energy is negligible, $\Delta G_{cav}(X_{sol} \rightarrow Y_{sol}) = G_{cav}(Y_{sol}) - G_{cav}(X_{sol}) \cong 0$. The correct procedure to calculate the $\Delta G_{sol}(X_{sol} \rightarrow Y_{sol})$ using QM calculations is through the solvation thermodynamic cycle discussed later on (Section 2.4) where the solvation free energy of X and Y are calculated.

The dipole moment and the atomic charge distributions were calculated for each solute with the geometry obtained in solution using the fitting of the QM electrostatic potential in solution with ChelpG (Charges from Electrostatic Potentials using a Grid based method) [35]. Therefore, for each solute a set of polarized atomic charges was obtained and the difference in the electronic energy due to the polarization of the solute in the presence of the solvent, $\Delta E_{pol}(X_{sol})$, was calculated as a difference of the solute electronic energy with a polarized wavefunction in solution with PCM, Ψ_{pol}, and in gas phase, Ψ_{gas}, $\Delta E_{pol}(X_{sol}) = \langle \Psi_{pol}|H_o|\Psi_{pol}\rangle - \langle \Psi_{gas}|H_o|\Psi_{gas}\rangle$, where H_o is the Hamiltonian of the isolated solute.

All the QM calculations were performed using the Gaussian 09 code [36].

2.2. Gas phase simulations

The gas phase simulations were performed with classical molecular mechanics using the Configurational Bias Monte Carlo (CBMC) method based on fragments [37] as implemented in the DICE program [38]. In CBMC, the molecule is divided in parts called fragments, and at each CBMC step the fragments are removed and reinserted with a different dihedral angle selected from a set of randomly selected trial angles, producing a new conformation which may be accepted or not according to the CBMC criterion. The molecule is treated in a semi-flexible model, i.e, the rotatable bonds defined by the torsional angles shown in red in Fig. 1 are flexible and change during the simulation, but the other degrees of freedom are kept rigid. More details on the CBMC implementation are given elsewhere [38,39].

We performed 1.5×10^7 CBMC production steps, simulations in the NVT ensemble, considering a single molecule in a cubic box with side of 70 Å at 298.15 K. We used 16 trial insertion angles at each CMBC step, obtaining an acceptance ratio of 60%. The Lennard-Jones parameters, ε and σ, were taken from the OPLS-AA [40] force field. The atomic charges were calculated at the CAM-B3LYP/cc-pVDZ level in vacuum fitting the QM electrostatic potential with the ChelpG method. The torsional potential around each rotatable bond was also taken from the OPLS-AA force field. The parametrization of the classical force field of each solute (X = DHA, VHF, DHA-DHA*p*, DHA-DHA*m*, DHA-VHF*p* and DHA-VHF*m*, shown in Fig. 1) is presented in the Supporting Information (SI) and was used for the gas phase and solute–solvent simulations.

2.3. Solute-solvent simulations

We keep the solvent molecules rigid and the solute is treated either rigid or semi-flexible as in the gas phase simulations. Preferential sampling [41] was used to select the solute and the surrounding solvent molecules more often in each simulation step. When the solute molecule is selected, 80% of the trials attempt intramolecular deformation changing the dihedral angles around the rotatable bonds, while 20% of the trials attempt translation of the center of mass and rotation around a randomly selected axis. We used 16 trial insertion angles were generated for each trial insertion, resulting in a CBMC acceptance ratio from 15% to 25%, depending on the solute molecule.

The simulations were performed on the isothermic-isobaric (NPT) ensemble. A cubic box composed of 1 solute X surrounded by 1000 acetonitrile molecules. Periodic boundary conditions and image method are used for the simulation box. The maximum displacement and rotation angle are adjusted to obtain an overall acceptance rate of 50%. We used the same force field that was employed in the gas phase simulation, but now with polarized atomic charges that were calculated at the CAM-B3LYP/cc-pVDZ level in acetonitrile solution (dielectric constant of 35.7 in PCM) fitting the QM electrostatic potential in solution with the ChelpG method. Therefore, the solute molecules considered in solution simulations were polarized by the solvent as described in previous successful studies [42,43]. The force filed used for acetonitrile molecules is the six-site model developed by Jorgensen and co-authors [44].

We started the simulation box in a random configuration and performed 1.0×10^8 CBMC steps for the thermalization stage. For production, 5.0×10^8 steps were performed. The temperature and pressure were 298.15 K and 1 atm, respectively. During the simulations the cubic box length fluctuates giving an average density of 0.758 ± 0.006 g/cm^3 in agreement with the experimental values of is 0.777 g/cm^3 [45]. The box length is ~ 45 Å and the cut-off-radius is ~ 22 Å for intermolecular interactions.

2.4. Free energy difference in solution

The stabilities of the isomers in acetonitrile solution were investigated using the solvation thermodynamic cycle to obtain the difference of the Gibbs free energy ΔG_{sol}(DHA→VHF) between the isomers DHA and VHF as

$$\Delta G_{sol}(\text{DHA} \rightarrow \text{VHF}) = \Delta G_{gas}(\text{DHA} \rightarrow \text{VHF}) + \Delta G_{solv}(\text{VHF}) - \Delta G_{solv}(\text{DHA}) \quad (1)$$

as well as their two DHA units molecules, DHA-DHA and DHA-VHF. In Equation (1) ΔG_{gas}(DHA→VHF) = G_{gas}(VHF) – G_{gas}(DHA) is the difference of the Gibbs free energy of the molecules in gas phase obtained with QM calculations (see Section 2.1) and the ΔG_{solv}(DHA) and ΔG_{solv}(VHF) are the solvation free energy of each molecule.

The solvation free energy ΔG_{solv} was calculated using Monte Carlo (MC) simulations with the Free Energy Perturbation method (FEP) [46,47] implemented in the DICE program. During these simulations both the solute and solvent molecule are kept rigid. We follow the Ben-Naim's definition [48] of the solvation free energy as the variation in the Gibbs free energy to bring a solute molecule from the gas phase to the solution. Here we considered the non-polarized solute in gas phase with X_{gas} geometry at the standard concentration condition of 1 M, used in most experimental data, and the polarized solute in acetonitrile solution with X_{sol} geometry at normal conditions of temperature and pressure (T = 298.15 K and P = 1 atm). Therefore the ΔG_{solv} was calculated adding four terms: (i) the free energy variation due to the change in the pressure of the gas phase from the standard concentration of 1 M (P_g = 24.46 atm) to the condition in equilibrium with the pressure of the solution (P_s = 1 atm), $\Delta G_p(P_g \rightarrow P_s)$; (ii) the variation of the solute energy due to the geometry change going from the gas phase to the solution, ΔE_{geom} obtained with QM calculations; (iii) the solute polarization energy due to the polarization process of the solute going from the gas phase to the solution, ΔE_{pol} obtained with QM calculations; and (iv) the solvation free energy due to the insertion of the polarized solute molecule in solution, $\Delta G_{sol}(0 \rightarrow$ DHA), that is equal to the negative of the solute annihilation free energy in solution [28,29], $\Delta G_{sol}(0 \rightarrow \text{DHA}) = -\Delta G_{sol}(\text{DHA} \rightarrow 0)$ obtained with FEP-MC simulations but also for comparison with QM calculation using the solvent as PCM. Then, in the case of the DHA molecule, we have

$$\Delta G_{solv}(\text{DHA}) = \Delta G_p(P_g \rightarrow P_s) + \Delta E_{geom}(\text{DHA}) + \Delta E_{pol}(\text{DHA}) - \Delta G_{sol}(\text{DHA} \rightarrow 0) \quad (2)$$

where the first term has the same value for all solutes, $\Delta G_p(P_g \rightarrow P_s) = -RT \ln(P_s/P_g) = -1.9$ kcal/mol; the second and the third terms were calculated as discussed in Section 2.1; and for the fourth term were calculated using the annihilation process in eleven FEP-MC simulations to make the polarized solute disappear slowly from the solution in three stages: first, 4 simulations with double-wide sampling to annihilate the Coulomb potential; next, 2 simulations with double-wide sampling to annihilate the attractive term of the LJ potential; and finally, 5 simulations with single-wide sampling to annihilate the repulsive term of the LJ potential. The procedure of the double-wide sampling and FEP-MC simulations are detailed in Refs. [28,29]. The sum of the results of the first stage, named $\Delta G_{\{q\}}$ with ΔE_{pol}, provides the electrostatic contribution to the solvation free energy, that is, $\Delta G_{solv\text{-}ele} = \Delta G_{\{q\}} + \Delta E_{pol}$. The remaining terms produced by the second and third stages ($\Delta G_{\{LJ\}}$) summed with ΔG_p and ΔE_{geom} are the non-electrostatic contribution to the solvation free energy $\Delta G_{solv\text{-}nonele} = \Delta G_{\{LJ\}} + \Delta G_p(P_g \rightarrow P_s) + \Delta E_{geom}$. The separation of the solvation free energy in these two terms ($\Delta G_{solv\text{-}ele}$ and $\Delta G_{solv\text{-}nonele}$) is interesting because it can be compared with those obtained using PCM model in QM calculations, although they are obtained based in different principles and approaches [34,49–51].

2.5. Theoretical spectroscopy in solution

The CBMC simulations generate a large number of configurations (or snapshots) which represents the solute conformer and the solution environment. We calculate the autocorrelation function of energy [21] and from it we define the interval between each snapshot necessary to produce statistically uncorrelated configurations. A reduced number of these configurations are sampled and submitted to quantum mechanical calculations of electronic spectra. The selected configurations are composed by one photochrome surrounded by the acetonitrile molecules. The number of acetonitrile molecules is chosen based on the solvation shells defined by the minimum-distance distribution function (MDDF) [52,53] that is more adequate for elongated solute than the radial distribution function (RDF). In the MDDF of the DHA-DHA and DHA-VHF dimers, the normalization used a parallelogram shape of the solute with the dimensions $24 \times 12 \times 6$ Å^3.

The quantum mechanical calculations were performed on these statistically uncorrelated configurations (a total of 100). The results of the excitation energies are given by simple numerical averages as well as by the convoluted spectra for the individual Lorentz distributions with line-width of 0.3 eV. These configurations represent many conformations of the solutes produced by the CBMC simulation and also the disordered solution environment. Therefore, the convolution of the spectra allows observing the inhomogeneous contribution to the band broadening caused by both liquid environment and flexibility of solute molecules.

2.6. Clustering analysis

To investigate the most stable conformers at room temperature and verify the solvent effects on the conformations of each solute, we obtained the distribution of the dihedral angles and also performed clustering analysis on the solute conformations obtained from the CBMC simulations in gas phase and acetonitrile solution. The clustering was performed using Clustering-Traj code [54], which uses the minimum RMSD found with the Kabsch algorithm [55] as the metric to evaluate the similarity of two structures. The clustering is performed with the average linkage method as implemented in SciPy [56]. A cutoff of 1.6 Å and 1.0 Å was used for the solute conformations in gas phase and in solution, respectively. These cutoffs showed a good compromise between the number of different clusters and the similarity of the structures. The analysis was performed on a set of 1000 statistically uncorrelated configurations of the solute extracted from the simulation.

3. Results

For the two units photochromic molecules, DHA-DHA and DHA-VHF, the nitrile groups can have two different orientations related to each other: in the same side or in the opposite side (up-down). We performed the geometry optimization in both rotamers for each molecule in gas phase and in acetonitrile with the PCM model.

The dihedral angles, the dipole moments and the differences of electronic energies due to the solvent effects in the geometry and in the polarization, ΔE_{geom} and ΔE_{pol} respectively, are shown in SI.

It was observed experimentally [13] by X-ray crystallographic the DHA-DHA*p* isomer with the nitrile groups in the opposite site (as illustrated in Fig. 1). Therefore, the further QM calculations presented in this work with optimized geometries were performed with the nitrile groups in opposite side.

3.1. Free energy of solvation

We summarize our results for the free energy of solvation in Table 1. The electrostatic and non-electrostatic terms are shown separately. Alongside each term, we give in parenthesis the results of calculations using the PCM model.

The electrostatic term, $\Delta G_{solv\text{-}ele}$, calculated with the FEP-MC simulations and PCM are in agreement, showing differences smaller than 1.0 kcal/mol. For the molecule DHA-DHA*p*, we obtained $\Delta G_{solv\text{-}ele}$ = −9.7 kcal/mol with FEP-MC and −9.4 kcal/mol with PCM. For its open form DHA-VHF*p*, $\Delta G_{solv\text{-}ele}$ = −12.9 kcal/mol was obtained with FEP-MC and −12.6 kcal/mol with PCM. In the MC simulations the electrostatic interactions between the molecules are described by the Coulomb potential. The atomic charges of solutes used in those simulations were calculated considering the polarization due to the PCM solvent model. Therefore, a good agreement between the electrostatic terms of the free energy of solvation $\Delta G_{solv\text{-}ele}$ is expected and observed in both models, as can be seen in Table 1. The agreement is not observed for $\Delta G_{solv\text{-}nonele}$, the non-electrostatic term. For the molecule DHA-DHA*p*, $\Delta G_{solv\text{-}nonele}$ = −36.4 kcal/mol was obtained with FEP-MC and 17.0 kcal/mol with PCM. For its open form DHA-VHF*p*, $\Delta G_{solv\text{-}nonele}$ = −35.3 kcal/mol with FEP-MC and 17.8 kcal/mol with PCM. The results for the non-electrostatic terms calculated using the continuum model are all positive. While in the PCM model this term corresponds to a parametrized contribution of the dispersion, repulsion and cavitation terms, in FEP-MC approach it is represented mostly by the Lennard-Jones potential in the simulations (see details in Computational procedure). The sum of the electrostatic and non-electrostatic terms is the total free energy of solvation $\Delta G_{solv} = \Delta G_{solv\text{-}ele} + \Delta G_{solv\text{-}nonele}$ in the last column of Table 1. In the case of DHA-DHA*p*, ΔG_{solv} = −46.1 kcal/mol was obtained with FEP-MC and 7.6 kcal/mol with PCM. For its open form DHA-VHF*p*, the FEP-MC and PCM provided ΔG_{solv} = −48.2 kcal/mol and 5.2 kcal/mol, respectively. For the PCM model all values of free energy of solvation are positive, contrary to the FEP-MC approach, which provides negative ΔG_{solv}. Therefore, only the theoretical results calculated with the FEP-MC ($\Delta G_{solv} < 0$) provides the right qualitative behavior for the free energy of solvation, as the PCM positive values would correspond to a non-solubility in acetonitrile. As we shall see below, all the experimental spectroscopic results to which we refer in this work are obtained in acetonitrile solvent. Therefore, they are soluble in acetonitrile and PCM fails in the calculations of ΔG_{solv} in acetonitrile.

To obtain the free energy difference to open the five carbon ring and convert DHA into VHF, using the solvation thermodynamic cycle (see Eq. (1)), it is necessary to calculate the difference of the free energy of solvation, $\Delta\Delta G$(VHF-DHA) = ΔG_{solv}(VHF) − ΔG_{solv}(DHA). These values are also in Table 1 in boldface. In the case of opening DHA-DHA*p* into DHA-VHF*p*, we obtained a $\Delta\Delta G$(-VHF-DHA) of −2.0 kcal/mol with FEP-MC and −2.4 kcal/mol with PCM. These values are influenced mostly by the electrostatic contribution of −3.2 kcal/mol obtained from both models than those originated from non-electrostatic contribution. For the $\Delta\Delta G$(VHF-DHA), both models presented an agreement with differences smaller than 0.5 kcal/mol. Therefore, the good results of the $\Delta\Delta G$ in acetonitrile obtained with PCM is due to an error cancellation since both isomers have similar volumes. Indeed, $\Delta G_{solv\text{-}nonele}$ = 17.0 kcal/mol for DHA-DHA*p* and 17.8 kcal/mol for DHA-VHF*p*.

Therefore, apart from the separated contributions (electrostatic/non-electrostatic), the overall agreement in the calculations of relative free energy of solvation shows an error cancellation in the PCM model. The calculated non-electrostatic terms in the open/-closed forms have similar values and when the difference is taken, it has no significant influence on the theoretical result of $\Delta\Delta G$(-VHF-DHA), providing the agreement in the two models for this difference but not for ΔG_{solv} of each molecule separately. We attribute the discrepancy between the non-electrostatic terms to the cavitation term obtained with the continuum and discrete models. The value provided by the PCM is significantly large in all molecules studied here and would be caused by the parametrization of the cavitation term for the acetonitrile solvent.

Table 2 presents the difference of free energy to open the five-membered ring in vacuum and in solution (see Eq. (1)). In solution both models agree and the values calculated for the free energy to convert DHA to VHF does not present a significant difference between the monomers (one unit DHA, ΔG_{sol}(DHA→VHF) = 4.1 kcal/mol with FEP-MC and 4.8 kcal/mol for PCM) and the dimers (two-units DHA, in the case of *para* isomer ΔG_{sol}(DHA → VHF) = 6.9 kcal/mol with FEP-MC and 6.4 kcal/mol for PCM). Table 2 also presents an alternative to calculate the ΔG_{sol}(DHA→VHF) in the PCM model which does not use the solvation thermodynamic cycle (values presented in bracket). In this method the ΔG_{sol}(DHA→VHF) is calculate using the direct value of the free energy of each component, G_{sol}(DHA) and G_{sol}(VHF), obtained in the vibrational frequencies calculation after the geometry optimization. Therefore, in this calculation only the electrostatic term is considered in the QM calculation and parametrized contributions are not used for dispersion, repulsion and cavitation. These values in bracket are also in good agreement with the FEP-MC values in parenthesis (see Table 2). For opening the 5-member ring of the DHA solute, we conclude that there is no significant gain in thermal release of energy for the back reaction when the monomers or dimers are considered, as only one ring is opened. The numerical results show that in solvent the release of energy is smaller than in gas phase by approximately 2.5 kcal/mol.

Table 1
Free energy of solvation ΔG_{solv} and its electrostatic and non-electrostatic terms (in kcal/mol) calculated with FEP-MC simulations and in parenthesis calculated with PCM/HF/6-31G(d)/UAHF. The differences between the solvation free energy to open the five member ring from DHA to VHF, $\Delta\Delta G$(VHF-DHA), are also shown.

Solute	$\Delta G_{solv\text{-}ele}$	$\Delta G_{solv\text{-}nonele}$	ΔG_{solv}
DHA	−4.9 (−5.5)	−16.3 (+9.7)	−21.2 (+4.2)
VHF	−8.2 (−8.7)	−16.0 (+10.3)	−24.2 (+1.6)
$\Delta\Delta G$(VHF-DHA)	**−3.3 (−3.2)**	**+0.3 (+0.6)**	**−3.0 (−2.6)**
DHA-DHA*p*	−9.7 (−9.4)	−36.4 (+17.0)	−46.1 (+7.6)
DHA-VHF*p*	−12.9 (−12.6)	−35.3 (+17.8)	−48.2 (+5.2)
$\Delta\Delta G$(VHF-DHA)	**−3.2 (−3.2)**	**+1.1 (+0.8)**	**−2.1 (−2.4)**
DHA-DHA*m*	−10.8 (−10.6)	−35.3 (+18.1)	−46.1 (+7.5)
DHA-VHF*m*	−13.7 (−14.3)	−35.0 (+18.6)	−48.7 (+4.3)
$\Delta\Delta G$(VHF-DHA)	**−2.9 (−3.7)**	**+0.3 (+0.5)**	**−2.6 (−3.2)**

Table 2
Difference of free energy (in kcal/mol) to open the five member ring from DHA to VHF in gas phase, ΔG_{gas}(DHA→VHF), and in solution, ΔG_{sol}(DHA→VHF), calculated using the solvation thermodynamic cycle with FEP-MC and PCM/HF/6-31G(d)/UAHF in parenthesis. In brackets the values calculated directly as ΔG_{sol}(DHA→VHF) = G_{sol}(VHF) − G_{sol}(DHA) with PCM/CAM-B3LYP/cc-pVDZ.

Solute		ΔG_{gas}(DHA→VHF)	ΔG_{sol}(DHA→VHF)
DHA	VHF	7.1	4.1 (4.8) [4.5]
DHA-DHA*p*	DHA- VHF*p*	9.0	6.9 (6.4) [6.0]
DHA-DHA*m*	DHA-VHF*m*	7.3	4.9 (4.7) [4.8]

3.2. Conformational analysis

We performed a clustering analysis of the DHA-DHA and DHA-VHF solutes in gas phase and in acetonitrile solution. For DHA-DHA (*para* and *meta*) two conformational clusters were identified showing the major conformation change in the relative orientation of the nitrile groups: in opposite side (up-down is the most frequent cluster) and in the same side (down-down is the less frequent cluster). In Fig. 2 the most representative conformations of the dominant cluster of each solute obtained in gas phase and in acetonitrile simulations are shown. In the SI all clusters are shown. For DHA-DHA*m* the nitrile groups in the opposite side appear 99.2% in gas phase and 91.5% in acetonitrile solution and for DHA-DHA*p* 97.4% in gas and 100% in solution. Although the solvent effects change the percentage of the conformational clusters, the geometries of the DHA-DHA isomers are similar and clearly one cluster is dominant with more than 90% of the conformation presenting the nitrile groups in opposite side (up-down), one DHA group almost planar with the aromatic link-ring (less than 5° on the dihedral angle) and the other DHA group rotated out-of-plane by maximum of ± 35°. This result is in agreement with the X-ray crystallographic data [13].

The additional degree of freedom of the DHA-VHF, introduced by the ring opening, reflects on a larger variability of conformational clusters for the DHA-VHF*p* and DHA-VHF*m* in gas phase and in solution. Five conformational clusters were identified for DHA-VHF*m* and four clusters for DHA-VHF*p*. For DHA-VHF*m* the nitrile groups in the opposite site (front-back) appear 40.9% in gas phase and 47.5% in acetonitrile solution and for DHA-VHF*p* 57.5% in gas and 44.2% in solution. The solvent effects in the geometries of the DHA-VHF isomers are much more complex, but a dominant trend can be observed in the conformations: the nitrile groups in opposite side (front-back), the DHA and the VHF groups are rotated out-of-plane in the gauche orientation in relation to the aromatic link-ring (around 60° or 120° on the dihedral angle) and nitrile groups in relation with the 7 member-ring present *cis* or *trans* forms, as shown in Fig. 2 for the DHA-VHF*m* in gas and acetonitrile, respectively. In acetonitrile solution the geometry of DHA-VHF (*para* and *meta*) presents a tendency to be in a more compact conformation than in gas phase.

The configurations selected for the further electronic structure calculations reflect this variability of conformers. However, we did not find any major effects of the solute conformer on the absorption spectra of the studied systems except for the band broadening.

3.3. Absorption spectroscopy

Our description of the electronic absorption spectra of the photochromes includes: (i) conformational effects, (ii) solvent effects, included by the electrostatic embedding (EE) of point charges on

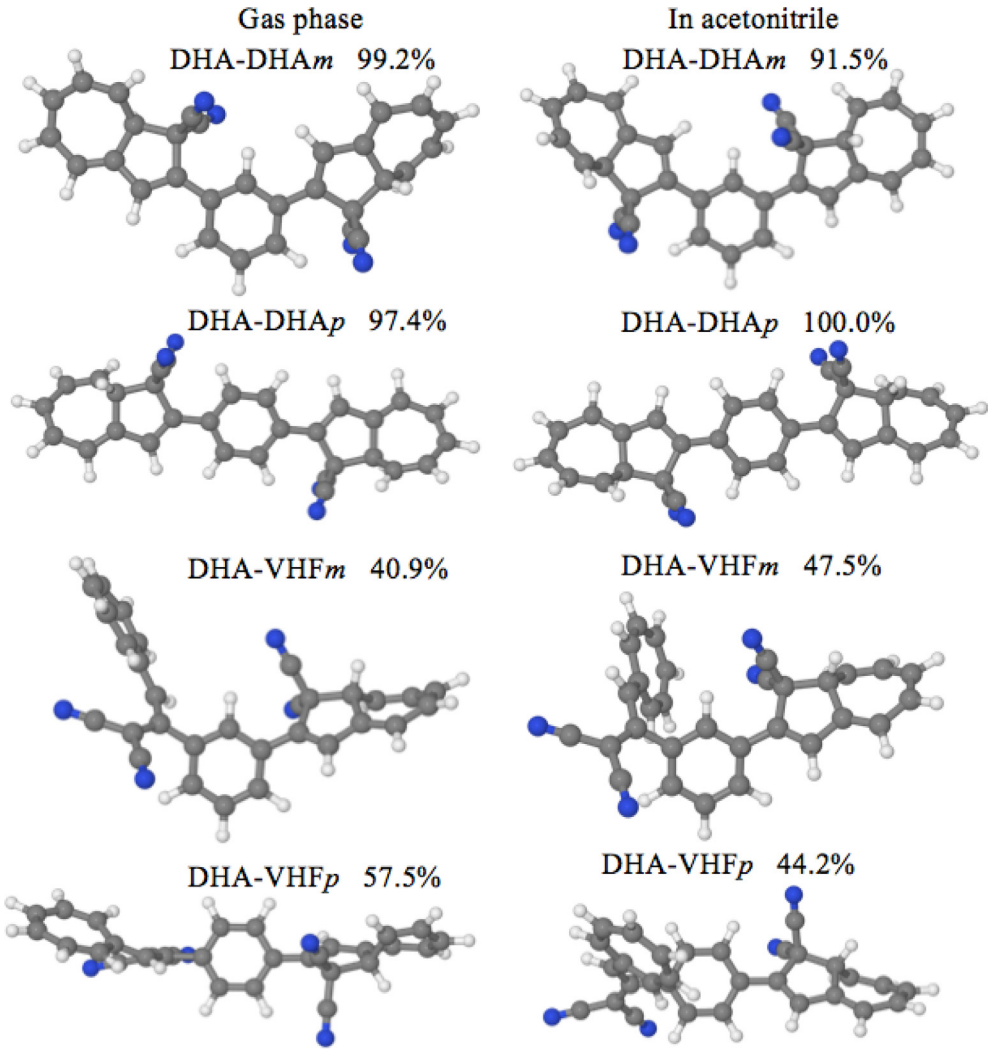

Fig. 2. Illustration of the most representative conformation of the dominant cluster and its occurrence (in percentage) for each solute obtained in gas phase and in acetonitrile simulations.

the positions of the solvent molecules and explicit solvent molecules plus the electrostatic embedding (ac + EE).

The analysis of the MDDF functions of each photochrome shows an equivalent distribution of solvent molecules around the solutes during the simulations. The graphics are presented in SI. The first solvation shell, up to ~ 4.25 Å, comprises a total of around 38 acetonitrile molecules. To consider all these solvent molecules explicitly in the QM calculations for the absorption spectra is computationally very demanding even using DFT, considering the amount of atoms (total of 280, being 52 of the solute) and basis functions (total of 2732, being 566 of the solute and 57 for each acetonitrile). We represent thus the model used for the calculations of the electronic absorption spectra of the photochrome in acetonitrile by including only a few nearest explicit solvent molecules (total of 8 acetonitrile molecules, 100 atoms and 1022 basis function), embedded in the electrostatic field of the remaining solvent molecules which corresponds to 500 acetonitrile molecules, corresponding to all solvent molecules until the edge of the simulation box. This is illustrated in Fig. 3. Therefore a set of 100 statistically uncorrelated configurations with 1 solute plus the electrostatic embedding of 500 acetonitrile molecules (S + EE) were also used to calculate the spectra and obtain a final average value.

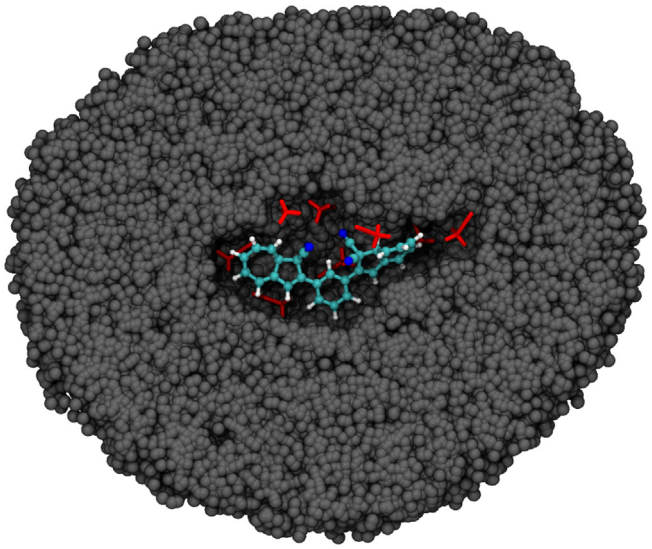

Fig. 3. Illustration of one configuration (S+8ac+EE) used in the QM calculation to obtain the excitation wavelengths. This configuration is composed by one solute DHA-DHA*m* surrounded by eight nearest explicit acetonitrile molecules (in red) embedded in the electrostatic field of the remaining solvent molecules (in black).

These 100 configurations represent the different conformers sampled during the CBMC simulation and reflect the conformational clusters as discussed above.

The intense transition of DHA-DHA*p* in its optimized geometry (gas phase) is calculated at 383 nm (Table 3). This excitation is well characterized as a HOMO-LUMO (Highest Occupied Molecular Orbital – Lowest Unoccupied Molecular Orbital) transition. In the isolated condition, the S_3 transition is well characterized as a HOMO-LUMO + 1 orbital promotion. All transitions shown can essentially be characterized by a four-orbital model comprising the two highest occupied and the two lowest unoccupied orbitals. The next two transitions are dipole forbidden and appear with zero intensity. A red shift is obtained when we consider the solvent effects of the electrostatic embedding plus the flexibility, both originated from the CBMC simulations. The low-lying transition in solvent is at 394 nm (red shifted by 11 nm (0.09 eV) compared to gas phase), and the next two transitions present a minor displacement, but the S_3 state becomes a weak intensity band at 280 nm when the solvent is included. The shift is in the correct direction towards the experimental result [12] (Table 3). The results for the DHA-VHF*p* molecule also in Table 3 show three low-lying states with some intensity in the gas phase calculation. In solvent, two separated bands are discernible with the S_1 being lowest in energy and the most intense located at 422 nm. The same shift of 11 nm is observed for this open form molecule. In fact, analyzing the values of the oscillator strengths, we noticed a reversal in the S_1 and S_2 states in solution. When DHA-VHF*p* is isolated, S_2 is the most intense transition with the large contribution provided from the HOMO to LUMO + 1 orbitals and some part of the HOMO to LUMO orbitals. However, in the solvent environment this is reversed and the S_1 state is the most intense transition characterizing the observed spectrum with the inversion also occurring for the orbitals, and now the HOMO to LUMO provides the major contribution. Thus, the red shift of the intense band, i.e. the shift between the calculate S_2 state in vacuum and the S_1 state in solvent, is actually larger, being 22 nm (or 0.17 eV). Contrary to DHA-DHA*p*, the DHA-VHF*p* changes its dipole moment from 6.5 D to 10.3 D upon solvation. Hence a larger solvatochromic shift is expected as indeed is obtained. The experimental absorption maximum [12] is difficult to ascertain in this case because it is composed of overlapping bands of the *para* isomers of DHA-DHA, DHA-VHF and VHF-VHF. Hence the experimental value is not provided in the Table 3.

Next we discuss the results obtained for the *meta* isomers. The calculated dipole moment for DHA-VHF*m* changes from 8.2 D in the isolated condition to value of 14.1 D in solvent, leading to a considerable electronic polarization due to the electrostatic embedding of the solvent. In the case of DHA-DHA*m* the dipole moment is calculated to increase from 4.7 D to 7.8 D from gas

Table 3
Electronic absorption excitation (in nm) and oscillator strengths (in parenthesis) of the photochrome optimized geometries and flexible conformations (in brackets). The solvent effects are included with the electrostatic embedding (S+EE) and with 8 explicit acetonitrile plus the electrostatic embedding (S+8ac+EE) over 100 statistically uncorrelated configurations obtained from the simulation. All the calculations were performed with TD-DFT using CAM-B3LYP/cc-pVDZ. Uncertainty is the standard deviation. The experimental data [12] are shown for comparison.

Solute	Exc.	λ(S)	⟨λ(S + EE)⟩	⟨λ(S + 8ac + EE)⟩	λ_{max} (Exp.)
DHA-DHA*p*	S_1	383 (1.29)	387 (1.31) [394 ± 5 (1.28)]	391 ± 3 (1.30)	408
	S_2	334 (0.00)	336 (0.00) [340 ± 2 (0.02)]	339 ± 3 (0.01)	–
	S_3	274 (0.00)	276 (0.33) [280 ± 2 (0.13)]	279 ± 3 (0.22)	–
DHA-VHF*p*	S_1	411 (0.14)	423 (0.696) [422 ± 5 (0.52)]	428 ± 3 (0.65)	–
	S_2	400 (0.61)	407 (0.080) [403 ± 7 (0.14)]	408 ± 7 (0.11)	–
	S_3	351 (0.57)	354 (0.573) [352 ± 13 (0.48)]	358 ± 4 (0.56)	–
DHA-DHA*m*	S_1	355 (0.71)	358 (0.71) [356 ± 5 (0.73)]	361 ± 3 (0.70)	365
	S_2	339 (0.25)	342 (0.26) [340 ± 6 (0.22)]	345 ± 3 (0.26)	–
	S_3	286 (0.00)	288 (0.00) [290 ± 3 (0.00)]	291 ± 3 (0.00)	–
DHA-VHF*m*	S_1	411 (0.10)	427 (0.58) [427 ± 5 (0.47)]	431 ± 3 (0.55)	476
	S_2	396 (0.49)	407 (0.10) [405 ± 6 (0.11)]	407 ± 7 (0.10)	–
	S_3	335 (0.42)	338 (0.43) [344 ± 9 (0.45)]	341 ± 2 (0.42)	360

phase to solution, respectively. In the DHA-DHA*m* the lowest state is relatively intense and characterizes the observed absorption band. The agreement with experiment is better for this isomer, which is 9 nm apart from the experimental value while the DHA-DHA*p* is 14 nm (see Table 3).

Interesting to note is again the relative change in intensity of the two lowest transitions obtained for DHA-VHF*m*, already observed in the case of DHA-VHF*p*. As Table 3 shows, for the isolated molecule the lowest transition obtained at 411 nm carries only a very weak intensity. In solvent the lowest transition is obtained as a more intense band as expected by experiment, and peaks at 427 nm, in comparison to experiment seen at 476 nm. The possibility of interchange between the calculated S_1 and S_2 states would imply a red shift of the isolated S_2 to solvated S_1 by 31 nm (0.23 eV) which is quite appreciable. However, it would also implies a small blue shift (~6 nm) of the π-π^* transition corresponding to the isolated S_1 to solvated S_2. Only in solvent it is obtained that the calculated lowest band at 427 nm is more intense than the next intense band calculated at 344 nm. This relative intensity is in due agreement with experiment [12] where the lowest energy band seen at 476 nm and located in the VHF part of the molecule is more intense than the other band seen at 360 nm and located in the DHA part. The lowest calculated transition is characterized by the HOMO-LUMO and HOMO-LUMO + 1 transitions with this latter orbital promotion showing a considerable charge transfer. The absorption of unit VHF is red shifted relative to the absorption in the DHA unit, as predicted in previous calculations [57] as well as experimentally [58–60].

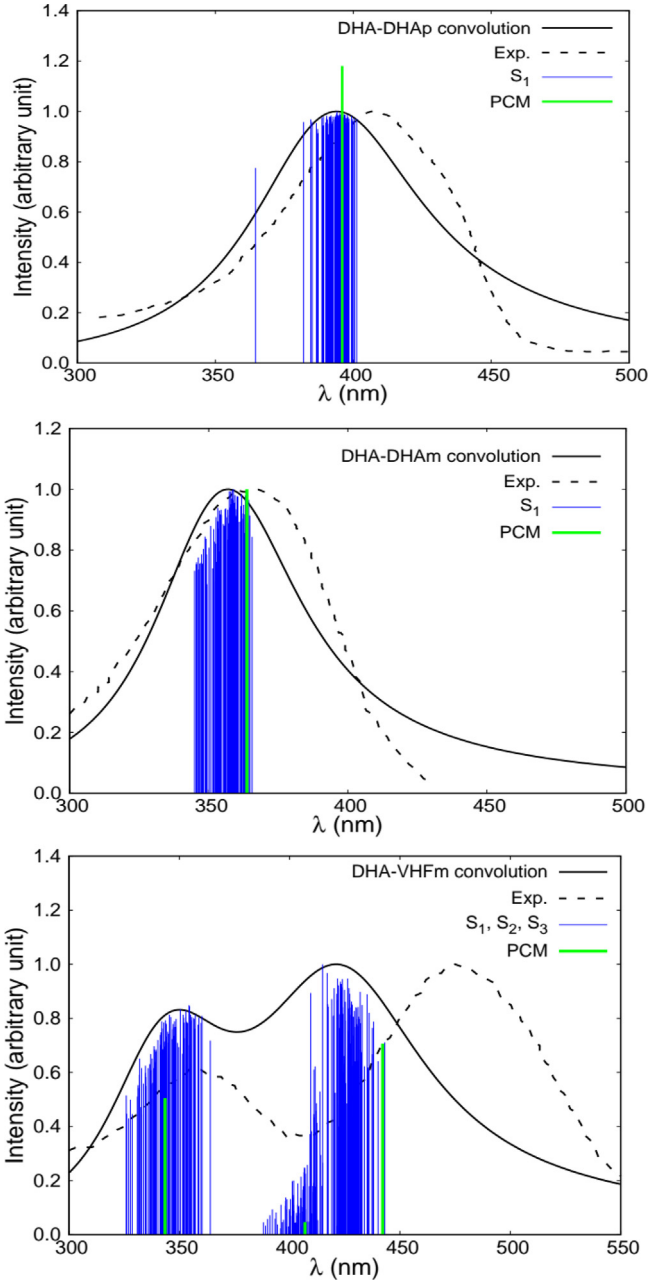

Fig. 4. Theoretical (vertical lines) and experimental [12] spectrum (dashed line) of the DHA-DHA*p* (top), DHA-DHA*m* (middle) and DHA-VHF*m* (bottom) in acetonitrile. The solid black line represents the theoretical results with convolution using an individual linewidth of 0.3 eV. In green the results calculated with PCM continuum model.

In Table 3 it is possible to see that the inclusion of 8 explicit nearest acetonitrile molecules plus the electrostatic embedding (S+8ac+EE) has only a small effect in the band shift. It typically contributes with a red shift of 3 or 4 nm in the intense excitation wavelength.

The broadening of the spectral band that originates from the solvent effects and flexibility is shown in Fig. 4. The first (top) convolution is the DHA-DHA*p* molecule and it presents a peak at 394 nm. The convoluted spectrum is composed of a total of 100 (the low-lying energy and most intense band) transitions and the corresponding oscillator strengths with individual line width of 0.3 eV. A general good agreement between theory and experiment can be observed indicating a proper representation of the observed experimental band. For comparison, the transition calculated using the PCM continuum model is also shown (Fig. 4, top), its value is 396 nm and it is located inside the standard deviation of the result obtained with the CBMC sampling of configurations. For the DHA-DHA*m* photochrome the first transition S_1 was also convoluted and is presented in Fig. 4 (middle). The PCM value for this case is in very good agreement with the experimental value, while the transitions calculated in the CBMC sampled configurations including the electrostatic embedding of charge points shows the natural broadening of the spectra. The three lower energy transitions of the DHA-VHF*m* photochrome are shown in the bottom of Fig. 4. The transition S_1, which shows its intensity only when calculated in solvent, and S_3 also with some intensity are well described in its shape and relative intensity between them as can be seen compared with the measured spectra.

4. Conclusions

A theoretical study of the absorption spectrum of photochromic molecules in solvent is presented. The multimode switch composed by a two DHA units of dihydroazulene (DHA)/vinylheptafulvene (VHF) molecule is considered in four possible isomers. Besides the spectroscopic study, the thermochemistry of these photochromic molecules is also presented with emphasis on its free energy of solvation using two solvent models. The free energy perturbation in Monte Carlo simulation (FEP-MC) method which considers the discrete nature of the solvent, and the continuum solvent PCM were used and the overall result shows an agreement between the models. On the other hand, it was noted that the non-electrostatic term is in large discrepancy between the two solvent models. We have attributed this disagreement to the cavitation term, which is included in the PCM model as a term that is parametrized for water. Another option for calculation of free energy differences ΔG_{sol} in acetonitrile is calculating the difference of the direct value of the free energy of each component, obtained in the vibrational frequencies calculation after the geometry optimization. Therefore, in this calculation only the electrostatic term

is considered in the QM calculation and none of the non-electrostatic terms is needed. For opening the 5-member ring of the DHA, we conclude that there is no significant gain in thermal release of energy for the back reaction when one or two DHA units are considered, as only one ring is opened. The numerical results show that in solvent the release of energy (~5 kcal/mol) is smaller than in gas phase (~7.5 kcal/mol). A clustering analysis of the CBMC simulations showed that the solvent has an effect on the dominant conformer in most cases, however, the different conformers do not introduce any major changes to the absorption spectra. The electronic absorption spectra in acetonitrile were calculated using TDDFT CAM-B3LYP/cc-pVDZ in solute–solvent configurations generated by the CBMC simulations. Compared to the isolated case the spectra of the different isomers in solvent are all red shifted. The influence of the solvent is also reflected in the relative intensities of the calculated transitions. Considering the statistically uncorrelated configurations and the solvent represented as point charges, the best agreement with experiment is within 0.1 eV. A good description of the inhomogeneous broadening of the spectra was obtained as a result of a sampling of both the conformational flexibility of the photochromes added to a discrete distribution of the solvent generated in molecular mechanics simulations.

Declaration of Competing Interest

The authors declare that they have no known competing financial interests or personal relationships that could have appeared to influence the work reported in this paper.

Acknowledgements

MHC thanks FAPESP for a postdoc fellowship, grant 2015/25249-7. HMC thanks the postdoc fellowship granted by CAPES from the BioMol project 23038.004630/2014-35. SC thanks CNPq grant 305203/2014-2. KC thanks CNPq grants 304371/2014-9 and 401187/2014-4. KC and SC thanks the National Institute of Science and Technology of Complex Fluids (INCT-Fcx) with the CNPq project 401187/2014-4 and FAPESP project no. 2014/50983-3 and also thanks CAPES for the BioMol project 23038.004630/2014-35. K.V.M. thanks the University of Copenhagen for financial support. SPAS thanks the Danish Agency for Science, Technology and Innovation for an International Network Programme grant 1370-00075B.

Appendix A. Supplementary data

Supplementary data (supporting information) to this article can be found online at https://doi.org/10.1016/j.saa.2021.119434.

References

[1] M. Irie, Y. Yokoyama, T. Seki (Eds.), New Frontiers in Photochromism, Springer, Tokyo, 2013.
[2] H. Dürrs, H. Bouas-Laurent (Eds.), Photochromism: Molecules and Systems, Elsevier, Amstersan, 2003.
[3] , Chem. Rev. 100 (2000) 5.
[4] B.L. Feringa (Ed.), Molecular Switches, Wiley, New York, 2001.
[5] T.J. Kucharski, Y. Tian, S. Akbulatov, R. Boulatov, Energy Environ. Sci. 4 (2011) 4449.
[6] J. Daub, T. Knochel, A. Mannschreck, Angew. Chem. Int. Ed. 23 (1984) 960.
[7] J. Ern, M. Petermann, T. Mrozek, J. Daub, K. Kuldová, C. Kryschi, Chem. Phys. 259 (2000) 331.
[8] H. Görner, C. Fischer, S. Giersisch, J. Daub, J. Phys. Chem. 97 (1993) 4110.
[9] H. Görner, C. Fischer, J. Daub, J. Photochem. Photobiol. A: Chem. 85 (1995) 217.
[10] N. Ree, M.H. Hansen, A.S. Gertsen, K.V. Mikkelsen, J. Phys. Chem. A. 121 (2017) 8856.
[11] M.H. Hansen, J. Elm, S.T. Olsen, A.N. Gejl, F.E. Storm, B.M. Frandsen, A.B. Skov, M.B. Nielsen, H.G. Kjaergaard, K.V. Mikkelsen, J. Phys. Chem. A 120 (2016) 9782.
[12] A.U. Petersen, S.L. Broman, S.T. Olsen, A.S. Hansen, L. Du, A. Kadziola, T. Hansen, H.G. Kjaergaard, K.V. Mikkelsen, M.B. Nielsen, Chem. Eur. J. 21 (2011) 3968.
[13] A. Vlasceanu, S.L. Broman, A.S. Hansen, A.B. Skov, M. Cacciarini, A. Kadziola, H. G. Kjaergaard, K.V. Mikkelsen, M.B. Nielsen, Chem. Eur. J. 22 (2016) 10796–10800.
[14] A. Vlasceanu, B.N. Frandsen, A.B. Skov, A.S. Hansen, M.G. Rasmussen, H.G. Kjaergaard, K.V. Mikkelsen, M.B. Nielsen, J. Org. Chem. 82 (2017) 10398–10407.
[15] A. Vlasceanu, M. Koerstz, A.B. Skov, K.V. Mikkelsen, M.B. Nielsen, Angew. Chem. Int. Ed. 57 (2018) 6069–6072.
[16] M.Å. Petersen, B. Rasmussen, N.N. Andersen, S.P.A. Sauer, M.B. Nielsen, S.R. Beeren, M. Pittelkow, Chem. Eur. J. 23 (2017) 17010–17016.
[17] M. Abedi, M. Pápai, K.V. Mikkelsen, N.E. Henriksen, K.B. Møller, J. Phys. Chem. Lett. 10 (2019) 3944–3949.
[18] M.H. Hansen, S.T. Olsen, K.O. Sylvester-Hvid, K.V. Mikkelsen, Chem. Phys. 519 (2019) 92–100.
[19] A.E. Hillers-Bendtsen, F.Ø. Kjeldal, K.V. Mikkelsen, Chem. Phys. Lett. 733 (2019) 136661.
[20] M.B. Nielsen, N. Ree, K.V. Mikkelsen, M. Cacciarini, Russ. Chem. Rev. 89 (2020) 573.
[21] K. Coutinho, S. Canuto, M.C. Zerner, J. Chem. Phys. 112 (2000) 9874.
[22] H.C. Georg, K. Coutinho, S. Canuto, J. Chem. Phys. 123 (2005) 124307.
[23] W.R. Rocha, V.M. Martins, K. Coutinho, S. Canuto, Theor. Chem. Acc. 108 (2002) 31.
[24] R. Rivelino, B.J.C. Cabral, K. Coutinho, S. Canuto, Chem. Phys. Lett. 407 (2005) 13.
[25] E.E. Fileti, K. Coutinho, T. Malaspina, S. Canuto, Phys. Rev. E 67 (2003) 061504.
[26] M. Hidalgo, S. Canuto, Phys. Lett. A 377 (2013) 1720.
[27] H.M. Cezar, S. Canuto, K. Coutinho, J. Mol. Liquids 307 (2020) 112924.
[28] R.C. Guedes, K. Coutinho, B.J.C. Cabral, S. Canuto, J. Phys. Chem. B 107 (2003) 4304.
[29] A.R. Cunha, E.L. Duarte, M.T. Lamy, K. Coutinho, Chem. Phys. 440 (2014) 69–79.
[30] T. Yanai, D.P. Tew, N.C. Handy, Chem. Phys. Lett. 393 (2004) 51–57.
[31] T.H. Dunning Jr., J. Chem. Phys. 90 (1989) 1007–1023.
[32] S. Miertuš, E. Scrocco, J. Tomasi, Chem. Phys. 55 (1981) 117.
[33] V. Baroni, M. Cossi, J. Tomasi, J. Chem. Phys. 107 (1997) 3210.
[34] J. Tomasi, Theor. Chem. Acc. 112 (2004) 184.
[35] C.M. Breneman, K.B. Wiberg, J. Comput. Chem. 11 (1990) 361.
[36] M.J. Frisch et al., Gaussian 09, Revision D.01, Gaussian Inc, Wallingford CT, 2013.
[37] J.K. Shah, E.J. Maginn, J. Chem. Phys. 135 (2011) 134121.
[38] H.M. Cezar, S. Canuto, K. Coutinho, J. Chem. Inf. Model 60 (2020) 3472.
[39] H.M. Cezar, S. Canuto, K. Coutinho, Int. J. Quantum Chem. 119 (2019) e25688.
[40] W.L. Jorgensen, D.S. Maxwell, J. Tirado-Rives, J. Am. Chem. Soc. 118 (1996) 11225.
[41] J.C. Owicki, Computer Modeling of Matter, American Chemical Society, Washington, 1978.
[42] V. Manzoni, M.L. Lyra, K. Coutinho, S. Canuto, J. Chem. Phys. 135 (2011) 144103–144111.
[43] V. Manzoni, M.L. Lyra, R.M. Gester, K. Coutinho, S. Canuto, Phys. Chem. Chem. Phys. 12 (2010) 14023.
[44] M.L.P. Price, D. Ostrovsky, W.L. Jorgensen, J. Comp. Chem. 22 (2001) 1340.
[45] X. Grabuleda, C. Jaime, P.A. Kollman, J. Comput. Chem. 21 (2000) 901.
[46] R.W. Zwanzig, J. Chem. Phys. 22 (1954) 1420.
[47] W.L. Jorgensen, K.J. Buckner, S. Boudon, J. Tirado-Rives, J. Chem. Phys. 89 (1988) 3742.
[48] A. Ben-Naim, Solvation Thermodynamics, Plenum Press, New York, 1987.
[49] J. Tomasi, M. Persico, Chem. Rev. 94 (1994) 2027–2094.
[50] J. Tomasi, B. Mennucci, R. Cammi, Chem. Rev. 105 (2000) 2999–3093.
[51] M. Orozco, F.J. Luque, Chem. Rev. 100 (2000) 4187–4225.
[52] H.C. Georg, K. Coutinho, S. Canuto, J. Chem. Phys. 126 (2007) 034507.
[53] S. Canuto, K. Coutinho, D. Trzesniak, Adv. Quantum Chem. 41 (2002) 161.
[54] H.M. Cezar, Clustering-Traj: Python code to analyze conformational clusters, (2019), GitHub repository, https://github.com/hmcezar/clustering-traj.
[55] W. Kabsch, Acta Crystallographica A32 (1976) 922.
[56] P. Virtanen, et al, SciPy 1.0 – Fundamental Algorithms for Scientific Computing in Python, 2019, preprint arXiv:1907.10121.
[57] S.T. Olsen, J. Elm, F.E. Storm, A.N. Gejl, A.S. Hansen, M.H. Hansen, J.H. Nikolajsen, M.B. Nielsen, H.G. Kjaergaard, K.V. Mikkelsen, J. Phys. Chem. A 119 (2015) 896.
[58] S.L. Broman, S.L. Brand, C.R. Parker, M.A. Petersen, C.G. Tortzen, A. Kadziola, K. Kilså, M.B. Nielsen, Arkivoc 9 (2011) 51.
[59] K. Fjelbye, T.N. Christensen, M. Jevric, S.L. Broman, A.U. Petersen, A. Kadziola, M.B. Nielsen, Eur. J. Org. Chem. 35 (2014) 7859.
[60] S.L. Broman, M.B. Nielsen, Phys. Chem. Chem. Phys. 16 (2014) 21172.